Superparamagnetic Iron Oxide Nanoparticles with Rigid Cross-linked Polyethylene Glycol Fumarate Coating for Application in Imaging and Drug Delivery

Morteza Mahmoudi,*,† Abdolreza Simchi,*,†,‡ Mohammad Imani,§ and Urs O. Häfeli||

Institute for Nanoscience and Nanotechnology, Sharif University of Technology, Tehran, Iran, Department of Materials Science and Engineering, Sharif University of Technology, Tehran, Iran, Novel Drug Delivery Systems Department, Iran Polymer and Petrochemical Institute, Tehran, Iran, Faculty of Pharmaceutical Sciences, University of British Columbia, Vancouver, British Columbia, Canada

Received: January 27, 2009; Revised Manuscript Received: March 9, 2009

Superparamagnetic iron oxide nanoparticles with proper surface coatings are increasingly being evaluated for clinical applications such as hyperthermia, drug delivery, magnetic resonance imaging, transfection, and cell/protein separation. To enhance the applicability of magnetic nanoparticles, two main problems must be overcome. First, as the drug coats the particle surface, a significant portion of it is quickly released upon injection (burst effect). Therefore, only small amounts of the drug reach the specific site after, for example, magnetic drug targeting. Second, once the surface-derivatized nanoparticles are inside the cells, the coating is likely digested, leaving the bare particles exposed to other cellular components and organelles, thereby potentially influencing the overall integrity of the cells. To overcome these two shortcomings, iron oxide nanoparticles with cross-linked poly (ethylene glycol)-co-fumarate (PEGF) coating were synthesized. The obtained material was highly stable and easy to handle due to the well-dispersed magnetic nanoparticles. Using the 3-(4,5-dimethylthiazol-2-yl)-2,5-diphenyltetrazolium bromide (MTT) assay, even very high concentrations of the novel magnetic nanoparticles were found to be biocompatible. To investigate if the coating could reduce the burst effect, nanoparticles were prepared by incorporating the anticancer drug tamoxifen. The cross-linked PEGF coating reduced the burst effect rate by 21% in comparison with the noncross-linked tamoxifen nanoparticles. Our results suggest that nanoparticles with coatings based on cross-linked unsaturated aliphatic polyesters are potentially useful to develop novel carriers for drug and gene delivery applications.

1. Introduction

The revolution in nanotechnology has brought us new tools not only in analytical systems but also for human applications. One of these new tools is magnetic nanoparticles (MNP).[1,2] Because of their ultrafine size, biocompatibility, and superparamagnetic properties, iron oxide nanoparticles are already approved for various biomedical applications such as enhanced resolution magnetic resonance imaging[3] and cellular labeling/cell separation[4−7] or undergoing preclinical and clinical evaluation for applications such as drug delivery,[8−14] tissue repair,[15] cell and tissue targeting,[16] and transfection.[17,18] Superparamagnetic iron oxide nanoparticles (SPIONs) with a mean particle diameter of about 10 nm suspended in appropriate carrier liquids are commonly called ferrofluids and have outstanding properties. Each particle contains only a single magnetic domain and can thus be treated as small, thermally agitated magnets in the carrier liquid. The special feature of ferrofluids is the combination of normal liquid behavior with superparamagnetic properties. This enables the use of magnetic forces for the control of properties and flow of the liquids, giving rise to numerous technical applications. Especially for in vivo applications, such as drug delivery, superparamagnetism is crucial because once the external magnetic field is removed, the magnetization disappears. Agglomeration, and hence the possible embolization of the capillary vessels, can thus not take place.[19] However, two major shortcomings encountered in the in vivo application of superparamagnetic particles include their destabilization due to the adsorption of plasma proteins and their nonspecific uptake by the reticulo-endothelial system (RES).[20,21] Because of the high specific surface area of the nanosized particles, plasma proteins interact with the particles, which can cause an increase in the particle size and often results in agglomeration. The particles are also considered as intruders by the innate immune system and can be readily recognized and engulfed by macrophage cells that may cause agglomeration. In both cases, the particles will be removed from the blood circulation, which will yield a decrease in their effectiveness, leading to a reduction in efficiency of nanoparticle-based diagnostics and therapeutics. To prevent both phenomena and provide longer circulation times, the particles are usually coated with hydrophilic and biocompatible polymers/molecules such as polyethylene glycol (PEG), dextran, polyvinyl alcohol (PVA), poly(acrylic acid), chitosan, pullulan, or poly(ethyleneimine) (PEI).[15,22] Furthermore, the immediate release of large amounts of the adsorbed/encapsulated drug (burst effect) upon application into the body, an effect that is related to the high surface-to-volume ratio of nanoparticles, will cause a reduction of the amount of drug that reaches the targeted site.

* To whom correspondence should be addressed. E-mail: mahmoudi@mehr.sharif.edu (M.M.); simchi@sharif.edu (A.S.).

† Institute for Nanoscience and Nanotechnology, Sharif University of Technology.

‡ Department of Materials Science and Engineering, Sharif University of Technology.

§ Novel Drug Delivery Systems Department, Iran Polymer and Petrochemical Institute.

|| Faculty of Pharmaceutical Sciences, University of British Columbia.

10.1021/jp900798r CCC: $40.75
Published on Web 04/16/2009

One possible strategy to overcome the difficult to control agglomeration and burst effect in SPIONs is to form an in situ hydrogel system. Unsaturated polyesters are suitable candidates to stabilize such a system by forming a cross-linked network via their unsaturated double bonds,[23−26] which can be cross-linked by photocuring or chemical methods. Fumaric acid containing macromers are highly unsaturated and can be cross-linked with or without using a cross-linking agent to form their corresponding polymeric networks.[27] Currently, a number of cross-linking agents, e.g., poly(propylene fumarate)-diacrylate (PPF-DA) and poly(ethylene glycol)-diacrylate (PEG-DA), are being used with fumaric acid containing macromers because they can enhance the polymerization efficiency while imparting specific properties to the network.[28]

The aim of the present work is to use cross-linked poly(ethylene glycol)-co-fumarate (PEGF) as a nanoparticle-coating hydrogel that will decrease protein interaction and reduce the burst effect. Very recently, He et al.[29] applied a similar coating (i.e., lactide-co-glycolide ethylene oxide fumarate) in order to either decrease the cytotoxicity effect of paclitaxel (a mitotic inhibitor used in cancer chemotherapy) or to increase its potential to evade the RES and target the drug to tumor vasculature. Consequently, it can be concluded that the PEGF family would be able to increase biocompatibility and decrease the avidity of the RES to remove the magnetic nanoparticles (MNP) from the blood circulation. To our knowledge, this polymer has not been used as a SPION coating yet.

2. Materials and Methods

2.1. Materials. Iron chloride and sodium hydroxide (NaOH) of analytical grades were supplied by Merck Inc. (Darmstadt, Germany) and used without further purification. PEG diol (MW 1 kDa), fumaryl chloride, calcium hydride, and propylene oxide were all purchased from Aldrich (Milwaukee, WI). Ammonium persulfate and methylene chloride (DCM) were obtained from Merck (Germany). Fumaryl chloride was purified by distillation at 161 °C under ambient pressure. Tamoxifen (TMX) was obtained from Pharma Chemie Company (Tehran, Iran). Anhydrous DCM was obtained by distillation under reflux condition for 1 h in the presence of calcium hydride. Other solvents were reagent grades and used without any further purification.

2.2. Synthesis of PEGF. PEGF macromer was synthesized by a slightly altered method of Temenoff et al.[25] (Scheme 1). Specifically, 0.03 mol of PEG diol was dissolved in 100 mL of anhydrous methylene chloride (DCM) in a three-necked 250 mL reaction flask equipped with a reflux condenser and a magnetic stirrer. Propylene oxide (PO), which is used as the catalyst and to bind the HCl produced during the polymerization, was added to the mixture in a 2:1 molar ratio. The purified fumaryl chloride (0.995:1 molar ratio to PEG) was dissolved in 50 mL of DCM and added dropwise in 1 h to the stirred reaction flask at −2 °C under nitrogen atmosphere. The reaction temperature was then raised to room temperature and run overnight. Upon completion of the reaction, the product was washed several times with 0.1 N NaOH to extract the byproducts such as chlorinated propanols. The PEGF macromer was then obtained by rotaevaporation, dried at 25 °C in vacuum for 24 h, and then stored at −15 °C until further use.

2.3. Synthesis of SPIONs Coated by PEGF. Solutions were prepared using deionized (DI) water after 30 min bubbling with argon for deoxygenation. The iron salts were dissolved in DI water containing 1 M HCl, where the mole fraction of Fe^{2+} to Fe^{3+} was adjusted to 2:1 for all samples. The precipitation was performed by dropwise addition of iron salt solutions to NaOH

SCHEME 1: Synthesis and Cross-linking of PEGF

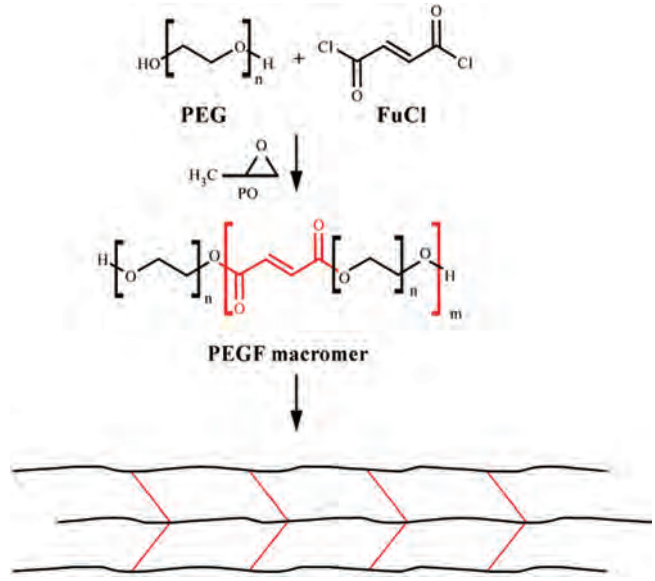

TABLE 1: Characteristics of Samples

name	core size (nm)	average hydrodynamic size (nm)	cross-linked
uncoated nanoparticles (MNP)	4	5 ± 2	
coated nanoparticles (PEGF-MNP)	5.1	12 ± 7	no
cross-linked coated nanoparticles (C-PEGF-MNP)	4.2	73 ± 34	yes

solutions under an argon atmosphere. To control mass transfer, which may allow particles to combine and build larger polycrystalline particles, turbulent flow was created by placing the reaction flask in an ultrasonic bath and changing the homogenization rates (in the first 2 min of the reaction). The molarity of the NaOH solution was 1.2. After 30 min, the solution was centrifuged at 10000*g* for 7 min and redispersed in DI water several times. Then PEGF solution, which was diluted in DI water, was added by syringe slowly (100 μL per drop) and kept stirring at 1000 rpm for 1 h in order to coat the surface of SPIONs. It is worthy to note that the PEGF/iron mass ratio was 2. The particles were collected by centrifugation at 10000*g* for 7 min and redispersed in DI water. Finally, unsaturated polyester coatings were cross-linked by redox polymerization in the presence of chemical initiators. Ammonium persulphate $[(NH_4)_2S_2O_8]$ as initiator system[30] and an optimized amount of accelerator (DMAEMA) were added and mixed thoroughly for 2 h. The ammonium persulphate/PEGF and DMAEMA/ammonium persulphate mass ratios were 0.02 and 0.1, respectively. The obtained ferrofluid was kept at 4 °C for future use. The MNP size characteristics are summarized in Table 1.

2.4. Methods. Morphology and size of the nanoparticles were investigated by TEM (ZEISS, EM-10C, Germany) operating at 100 kV and SEM (Philips-XL30) after placing and drying a drop of the suspension on a copper grid. Fourier transform infrared (FTIR) spectra (4000−400 cm^{-1}) were obtained on a Bruker Equinox 55 spectrophotometer at 4 cm^{-1} resolution and 32 scans. All samples were prepared as KBr discs. ^1H NMR spectra were recorded in $CDCl_3$ at 25 °C (Bruker Ultrashield 400 MHz, Germany). Phase characterization was accomplished using a XRD (Siemens, D5000, Germany) technique with Cu Kα radiation and Scherrer method for particle size determination. XRD samples were prepared by drying the obtained

particles in a vacuum oven at 40 °C for 12 h after centrifugation. The magnetization of the particles was measured in a vibrating sample magnetometer (VSM) with a sensitivity of 10^{-3} emu and magnetic field up to 20 kOe. The magnetic field was changed uniformly at a rate of 66 Oe/s. Thermogravimetric analysis (TGA) measurements were performed with a TGA thermal analysis system (SDT Q600, USA). The mass loss of the dried samples was monitored under an inert atmosphere (argon gas) from 30 to 500 °C at a rate of 5 °C min^{-1}.

2.5. Drug Release Studies. Tamoxifen (TMX), an antiestrogen drug used to treat breast cancer, was selected as antiestrogen drug.[31] The same amount of noncross-linked PEGF MNP and cross-linked PEGF MNP (confirmed by atomic absorption) were dried in vacuum. PBS pH 7.4 containing 1 mg of drug per mL was added to the dried materials and a stable colloidal suspension formed by dispersion of nanoparticles with a homogenizer at 10000 rpm as well as in an ultrasonic bath. After 10 h of incubation, MNP were collected via centrifugation at 10000*g* and dispersed in fresh PBS. Release data were collected for 300 min. Then 2 mL of each sample was centrifuged at selected times and the drug concentration measured in the supernatant using a UV spectrometer (Milton Roy Spectronic 601) at 277 nm. The TMX calibration curve was determined from 5−50 μg/mL in PBS pH 7.4. To estimate the amount of drug adsorbed to the surface of the SPION, the concentration of TMX in PBS solution was measured before and after interaction with SPION by UV spectrometry. The difference between the obtained amounts was taken as drug uptake by the SPION. All release and adsorption measurements were done in triplicates and the standard deviations calculated.

2.6. In Vitro Biocompatibility Assessment. Primary adherent mouse fibroblasts (L929) and human suspension leukemia cells (K562) from the National Cell Bank of Iran (NCBI), Pasteur Institute, were seeded on glass coverslips in 96-well plates at 10000 cells per well in 150 μL of medium and incubated for 24 h. Cells were cultured in Dulbecco's modified Eagle's medium (DMEM) supplemented with 10% fetal bovine serum (FBS) at 37 °C in a 5% CO_2 incubator. After the 24 h incubation period, 40 μL of medium containing SPIONs (5, 10, 20, 40, 50, 100, 200, 400, 800, and 1600 mM iron, measured by atomic absorption) was added to the wells, and cells were incubated for additional periods ranging from 24−48 h. Control cells were incubated with the same culture medium without particles. All particle concentrations and controls were each seeded in five separate wells.

Cytotoxicity was assessed using the MTT (3-(4,5-dimethylthiazol-2-yl)-2,5-diphenyltetrazolium bromide) assay, which is a nonradioactive, colorimetric assay.[32] After 24 and 48 h of incubation with the cell-SPION samples, 100 μL of MTT (0.5 mg/mL) was added to each well. Following incubation, the medium was removed and formazan crystals were solubilized by incubation for 20 min in 150 μL of isopropyl alcohol. The absorbance of each well, which assesses viable cells, was read at 545 nm on a microplate reader (Stat Fax-2100, Awareness, Palm City, FL).

Because published reports confirm that use of the MTT assay for measuring the toxicity of magnetite nanoparticles has high variability and nonspecificity,[33] the outlier detection method was applied to minimize variability. Cell detachment upon physical contact with SPIONs also necessitated the development of customized protocols for the MTT assay; detachment increased with both increasing SPION concentration and contact time.[34] In reducing the adhesive properties of L929 cells, SPION exposure may have increased error in the MTT assay through the elimination of crystals during removal of the supernatant. To accommodate for these cell detachment effects, cells were examined by optical microscopy to ascertain the density of violet spots prior to detachment. The supernatant was then carefully removed to quantify precipitated formazan. For samples exposed to SPION concentrations of 1600 mM over 48 h, cell detachment occurred prior to MTT addition. This required a reduction in the MTT incubation time to about 2 h to avoid cell detachment.

2.7. Outlier Detection. All MTT experiments were performed in triplicate or more, with the results expressed as mean ± standard deviation. The standard deviation values are indicated as error bars in the MTT results plots. The results were statistically processed for outlier detection using a "T procedure"[35] using MINITAB software (Minitab Inc., State College, PA). One-way analysis of variance (ANOVA) with $p < 0.05$ was performed for each set of MTT assay test repeats. Outlier samples have then been excluded from the corresponding assay viability calculations.

3. Results and Discussion

3.1. PEGF Characterization. The FTIR spectrum of the synthesized PEGF (Figure 1) is characteristic of the crystalline phase of PEG (absorption bands presented at 950 and 858 cm^{-1}); asymmetrical C−O−C stretching band, C═C stretching at 1645 cm^{-1}, carbonyl stretching, strong methylene absorption at 2871 cm^{-1}, methylene scissoring and asymmetric bending at 1455 cm^{-1}, and hydroxyl absorption are evident and can be found.

The ^{1}H NMR spectrum of the synthesized PEGF macromers with a chemical shift at 6.8 ppm clearly indicates that fumarate groups are incorporated into PEG (Figure 2). The chemical shifts with peak positions at 3.63, 4.33, 2.7, and 6.8 ppm are due to the protons of PEG main ethylene (b), methylene groups adjacent to the fumarate groups (c), the hydroxyl group of PEG (d), and hydrogens of the fumarate group (a), respectively.

3.2. PEGF-Coated MNP. Transmission electron microscopy (TEM) and scanning electron microscopy (SEM) of magnetite nanoparticles (Figure 3) reveals spherically shaped iron oxide nanoparticles with a narrow size distribution (Table 1). From Figure 3, we concluded that PEGF has been cross-linked; the obtained particles may be used as promising candidates for drug delivery and imaging due to the cross-linked coating. The proposed mechanism of the formation of a cross-linked shell on the surface of single SPION and magnetic beads (e.g., Figure 3d) is shown in Figures 4 and 5, respectively. It is worthy to note that no precipitation formed in the suspension of PEGF-coated SPION, not even after storage for more than six months, which is the maximum time period that other coatings, such as PVA,[34] are able to stabilize SPIONs. The high stability of PEGF-coated SPION is very likely due to the hydrogel property of PEGF, which is able to absorb water and decreases the density of the core−shell nanoparticles. In addition, the hydrogel coating is able to take up and release drugs due to their response to physical and chemical environment changes (e.g., pH and temperature, which can change the hydrogel properties), which make them novel in comparison to other coatings.[36]

Figure 6 shows examples of XRD spectra for bare magnetic nanoparticles (MNP), noncross-linked PEGF coated magnetic nanoparticles (PEGF-MNP), and cross-linked PEGF coated magnetic nanoparticles (C-PEGF-MNP). Small traces of Fe_2O_3 (maghemite) were observed in PEGF-MNP sample (see Figure 6; the peak is reflected by (104) plane of α-Fe_2O_3).[37,38] The XRD spectra are affected by the particle size and also by the magnetite content, both which are influenced by the operating parameters.

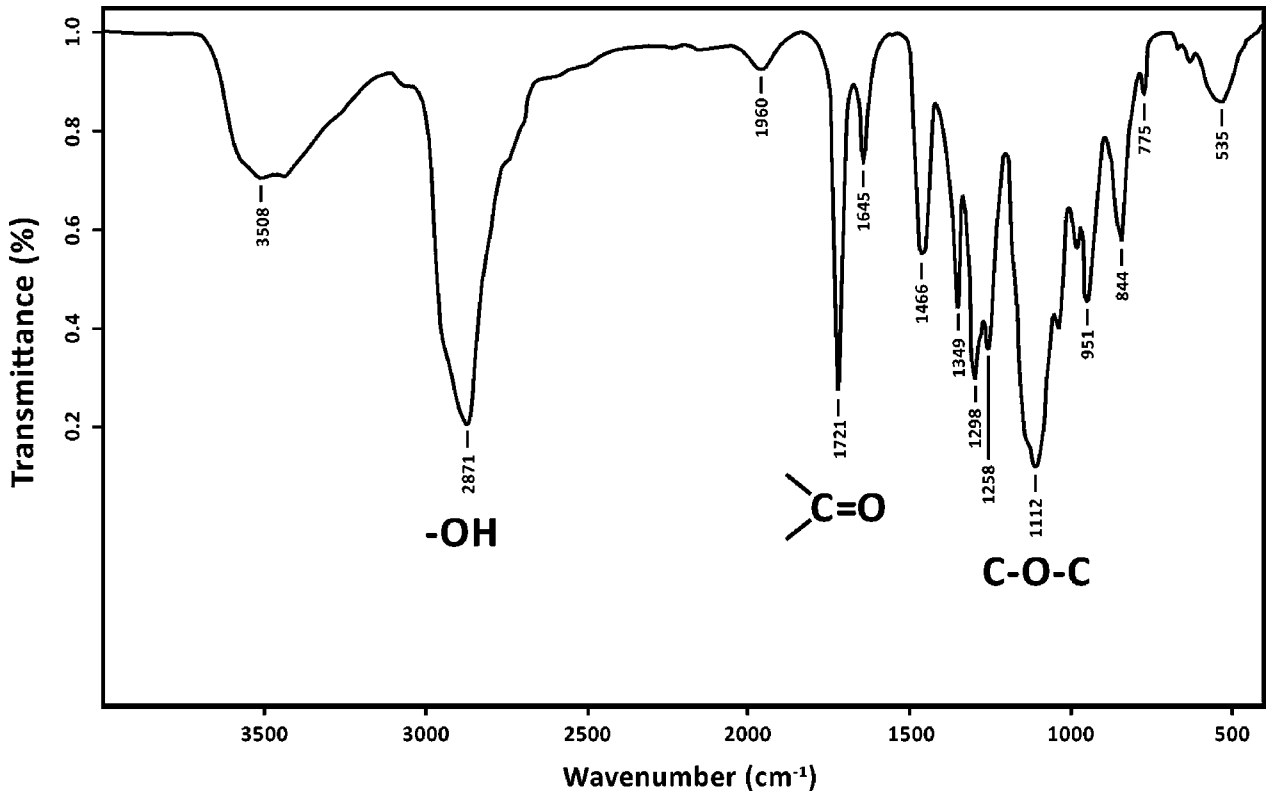

Figure 1. The FTIR spectrum of PEGF.

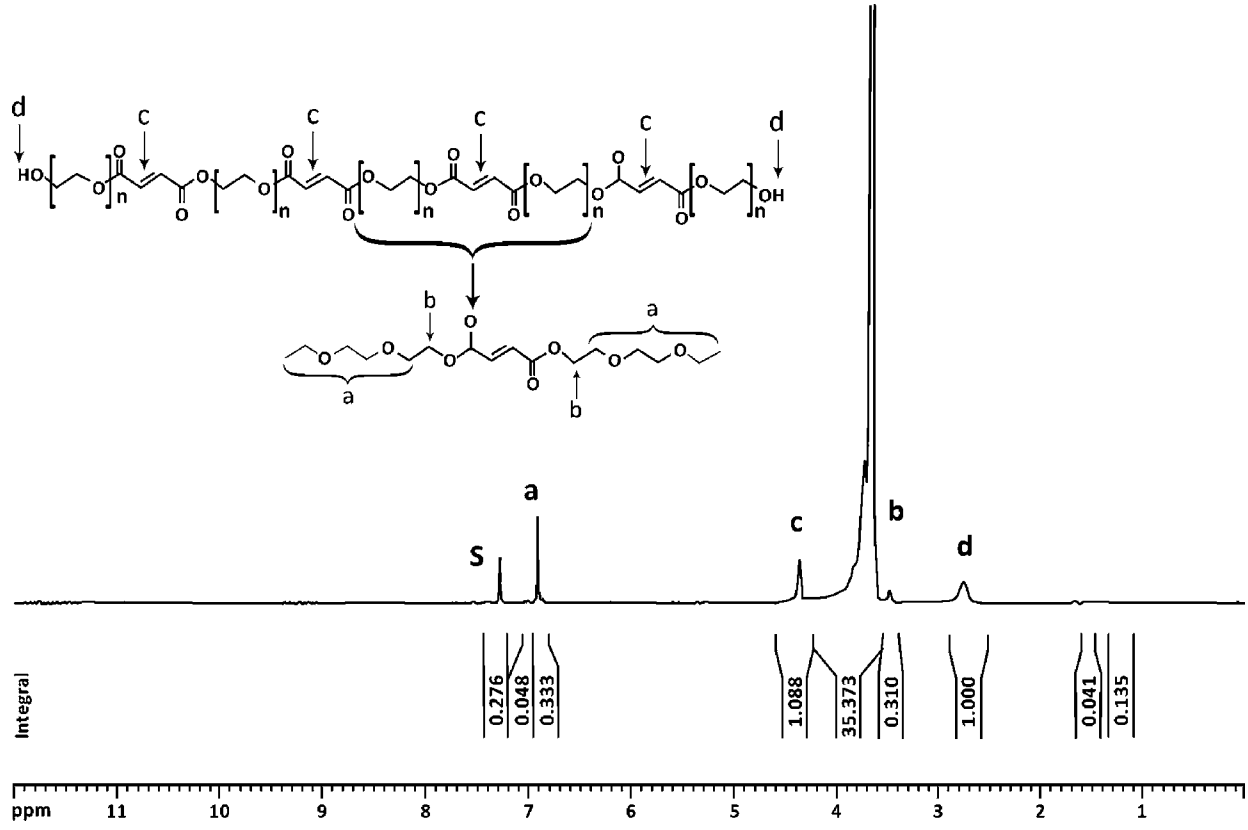

Figure 2. ^{1}H NMR spectrum of PEGF.

A possible mechanism of maghemite formation is the generation of bubbles in the reaction solution due to the use of high stirring rates and the effect of the ultrasonic bath, which may cause magnetite to be oxidized.[39]

The full width at half-maximum (fwhm) of the (311) reflection was used to determine the average crystallite size of the nanoparticles by using the Scherrer method. The obtained average core sizes via mentioned method were 4, 5.1, and 5 nm for MNP, PEGF-MNP, and C-PEGF-MNP, respectively.

The samples were analyzed by VSM and showed superparamagnetic behavior with different magnetic saturations (Figure 7). Remanence and coercivity in the hysteresis loops were

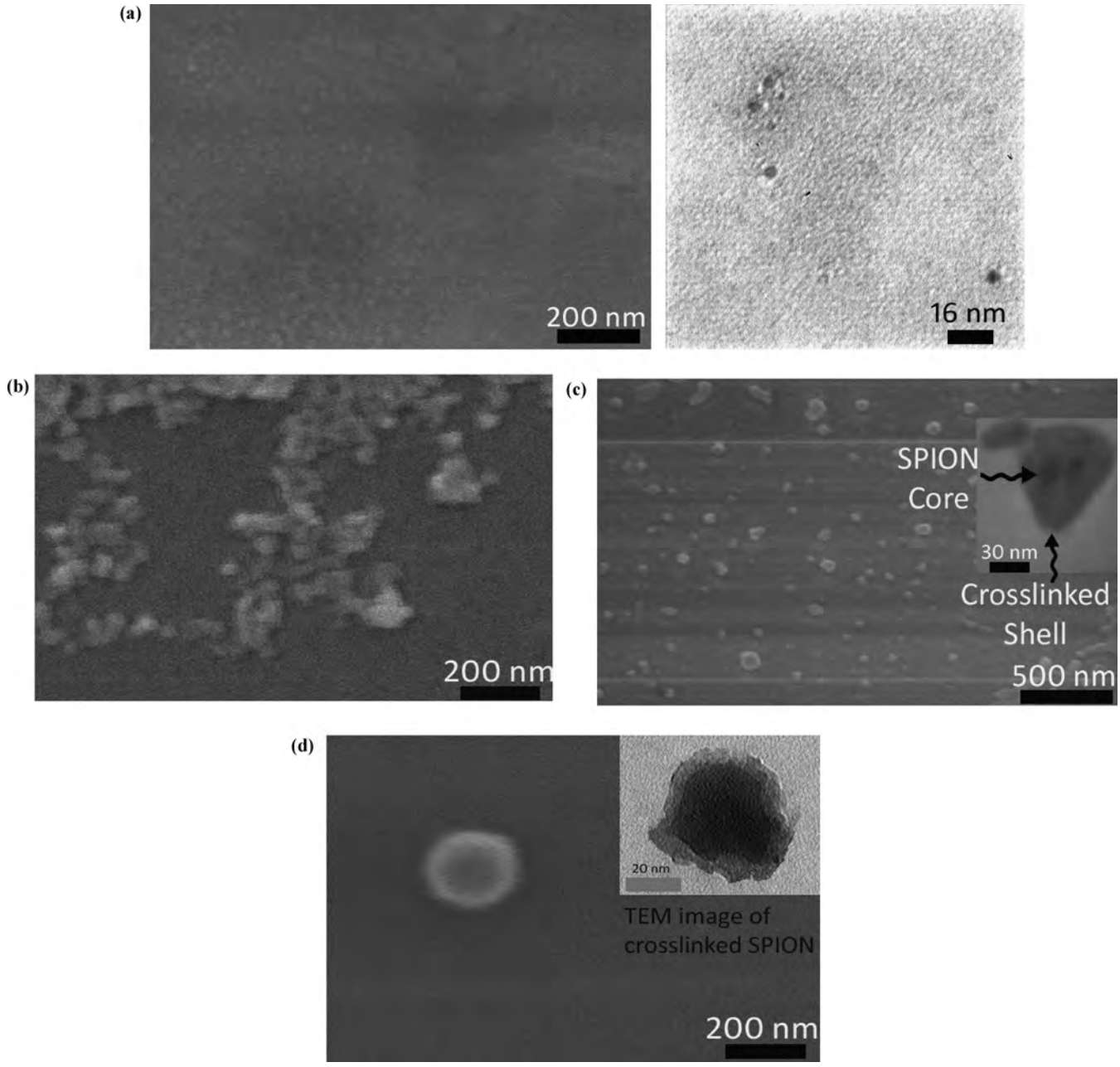

Figure 3. (a) SEM (left) and TEM (right) images of PEGF-MNP. (b) SEM image of C-PEGF-MNP. SEM and TEM images of (c) selected C-PEGF particles and (d) selected beads.

negligible. The magnetic particles reported in Table 1 are thus agglomerates of many magnetic nanoparticles in a polymer particle and do not consist of single magnetic beads, as such a bead would be ferromagnetic above a diameter of 27−30 nm.

Several researchers have reported that the magnetic saturation of superparamagnetic magnetite increases when the size of the magnetite increases, which can be attributed to the increase of weight and volume of magnetite nanoparticles.[39,40] According to these studies, the magnetic properties are lower than that of the bulk phase, which is 88 emu/g.[41−43] Considering the above-mentioned literature reports, the magnetic saturation is expected to increase due to increase in the size; however, Figure 7 clearly reveals that the existence of magnetic beads consisting of larger primary particles decreases the magnetic saturation in comparison with individual smaller nanoparticles due to the random dispersion of nanoparticles in polymeric beads, which may cause a decline in exchange penetration as well as dipolar interactions.[44] The average size of the particle can be estimated from the room temperature $M(H)$ curve using the slope near zero field ($H = 0$) according to the equation:[45]

$$V = \frac{\mathrm{d}M}{\mathrm{d}H}\frac{3kT}{M_s^2}\frac{\rho_c}{\rho_m}\frac{c}{c+1}$$

where V is the average volume of the particle, k is the Boltzmann constant, $c = \rho(\text{Fe oxide})/\rho(\text{PEGF})$, and ρ_c and ρ_m are the densities of the composite (e.g., PEGF coated SPION) and the pure magnetic material (e.g., MNP), respectively. Taking the maximum measured value of the composite magnetization as magnetic saturation and assuming the spherical shape of the particle, we have obtained the values of average particle diameter with computational method for the MNP, PEGF-MNP, and C-PEGF-MNP as 4.1, 4.2, and 3 nm, respectively. Theoretically, the estimated particle sizes from this equation would be decreased by the formation of cross-linked

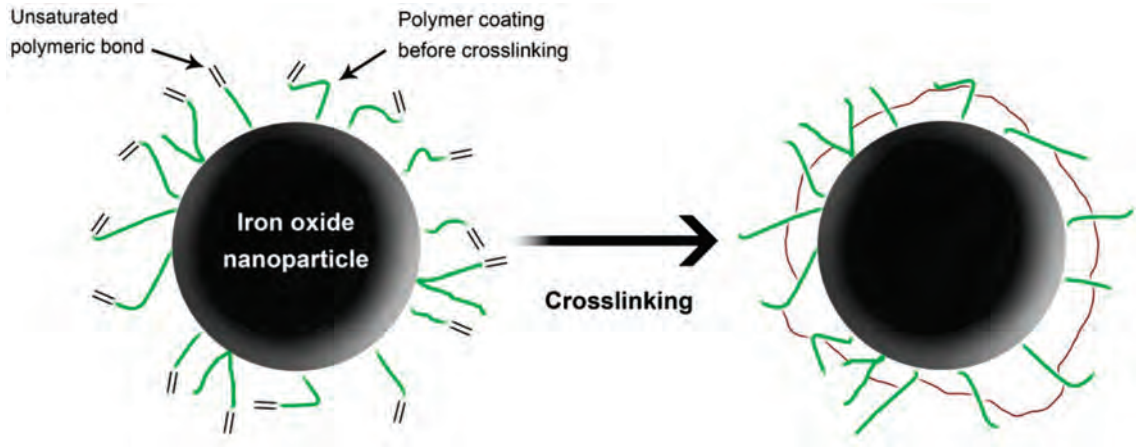

Figure 4. Proposed scheme of cross-linking PEGF that coats the iron oxide nanoparticles.

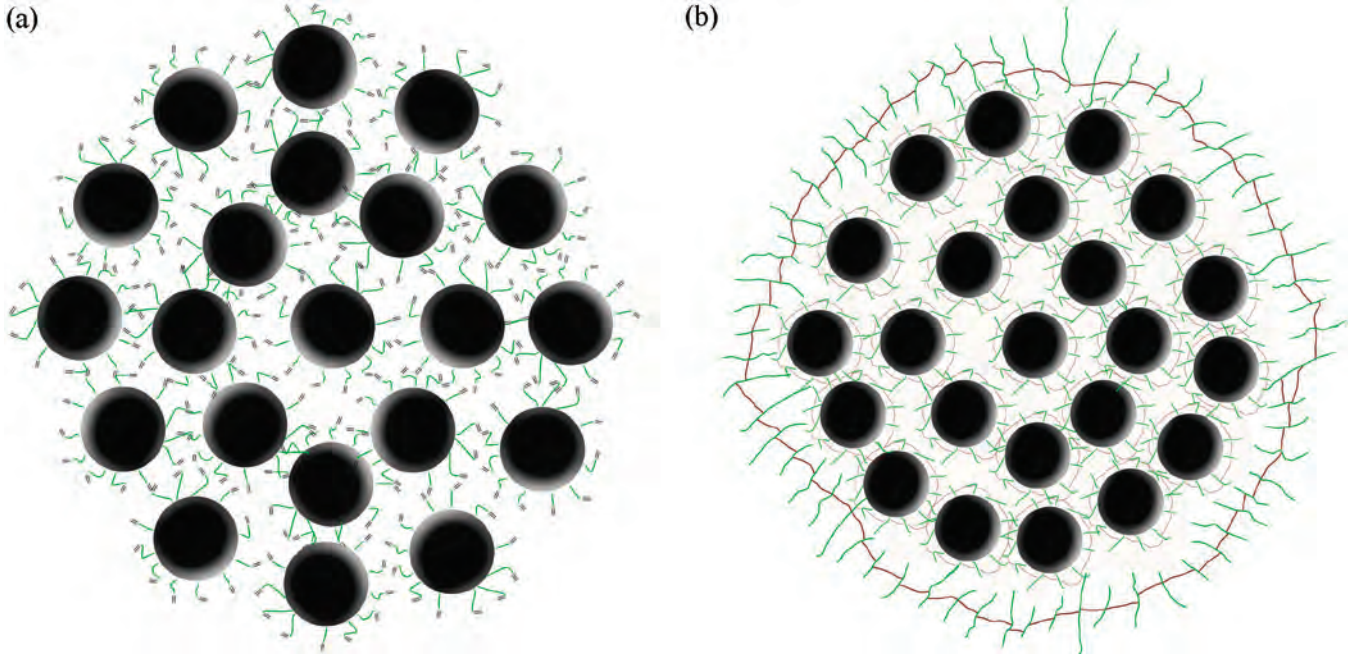

Figure 5. Proposed mechanism (a) before and (b) after cross-linking of magnetic beads.

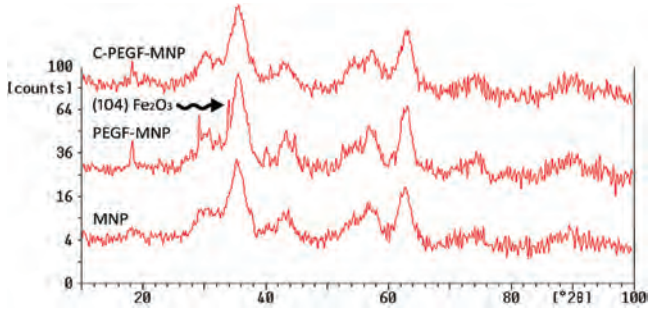

Figure 6. XRD patterns of (a) MNP, (b) PEGF-MNP, and (c) C-PEGF-MNP.

polymeric coating. The decline in magnetic saturation is significant for the cross-linked bead MNP (see Figure 5b). A possible explanation for this decline of magnetic saturation in cross-linked nanoparticles may relate to the lower amount of iron (i.e., because magnetite is replaced by the nonmagnetic polymer) rather than magnetocrystalline anisotropy. Because the cross-linked magnetic beads (Figure 8b) cannot move to their easy axes directions, the net magnetization is decreased in comparison with noncross-linked ones (Figure 8).

Figure 9 shows the FTIR spectra of PEGF-coated MNP before and after cross-linking. The FTIR spectrum of iron oxide exhibits strong bands in the low-frequency region (1000−500 cm^{-1}) due to the iron oxide skeleton. This pattern is consistent with the magnetite (Fe_3O_4) spectrum (band between 570−580 cm^{-1}) or the maghemite (γ-Fe_2O_3) spectrum (broad band 520−610 cm^{-1}).[46] The characteristic band of Fe−O at 572 cm^{-1} shows that the particles consist mainly of Fe_3O_4.

On the spectra of the macromers, the characteristic ester carbonyl stretching bond at 1721 cm^{-1}, asymmetrical C−O−C stretching bond at 1110 cm^{-1}, C−H stretching bond at 2869 cm^{-1}, C═C stretching bond at 1644 cm^{-1}, methylene scissoring, and asymmetric peaks at 1454 cm^{-1} were detected. According to the FTIR spectra, the macromers showed mostly terminal fumarate carboxyl functional groups, which are evident by the weakening of the broad −OH end groups absorption at 3500 cm^{-1}. The FTIR in Figure 9 proves that PEGF has been cross-linked, as the number of unsaturated bonds has decreased significantly. Results of thermogravimetric analysis on the PEGF-MNP and C-PEGF-MNP shown in Figure 10 also support the notion that PEGF was cross-linked. A bigger mass loss is observed for the PEGF-MNP in contrast to C-PEGF-MNP. The

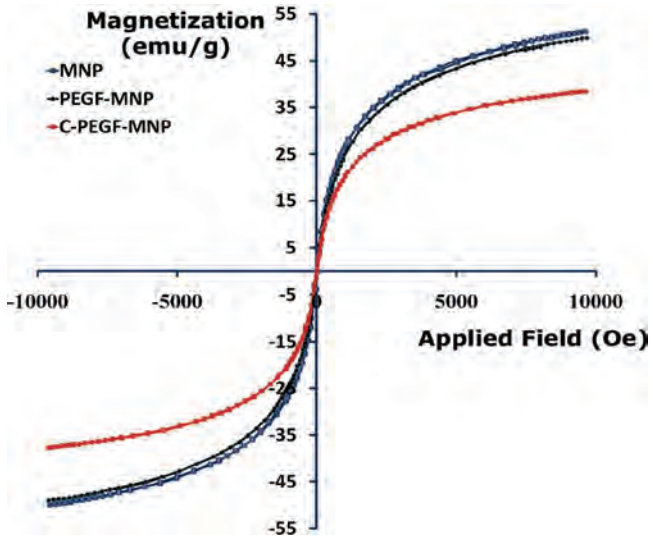

Figure 7. Magnetization curves for (a) MNP, (b) PEGF-MNP, and (c) C-PEGF-MNP.

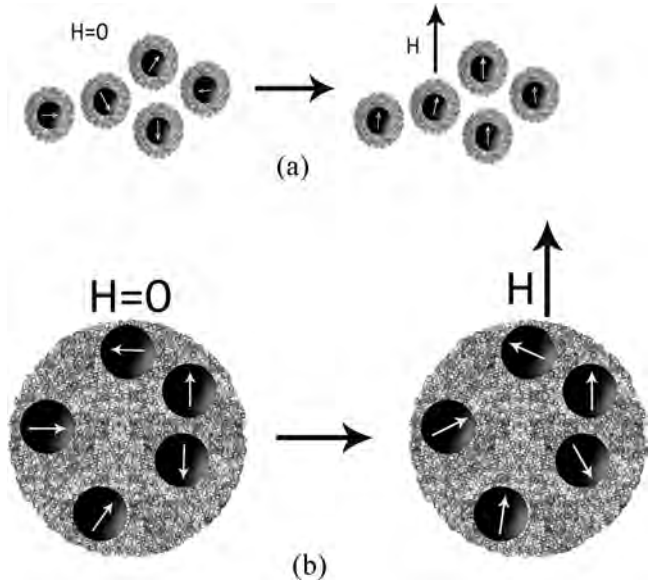

Figure 8. Scheme of net magnetization for (a) single MNP and (b) beads MNP.

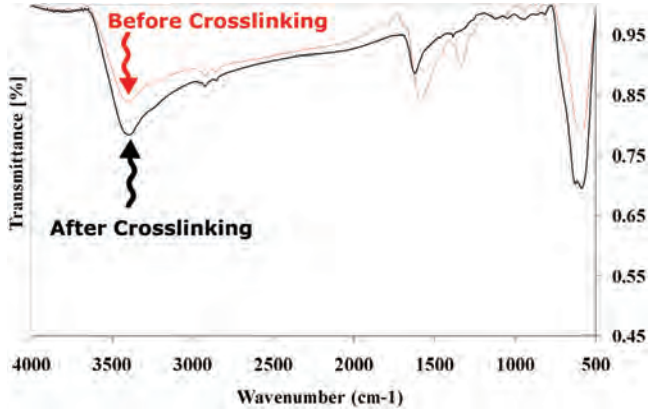

Figure 9. FTIR spectrum of PEGF coated SPION before and after cross-linking.

lower decreasing slope for the PEGF-MNP very likely is due to its cross-linked matrix.

3.3. Release Studies. Figure 11 illustrates drug release from PEGF-MNP and C-PEGF-MNP. Both MNP systems showed

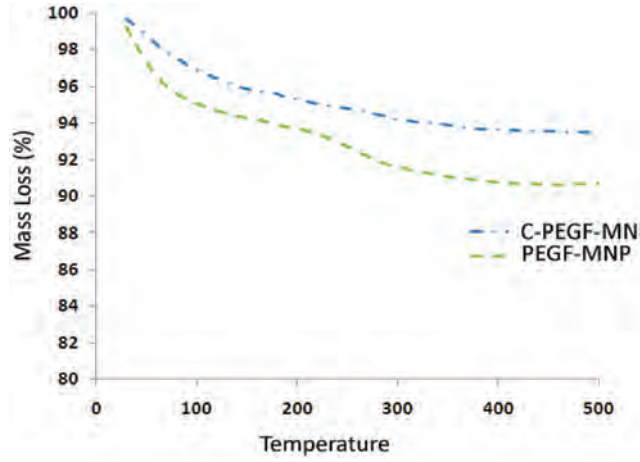

Figure 10. TGA results for PEGF-MNP and C-PEGF-MNP.

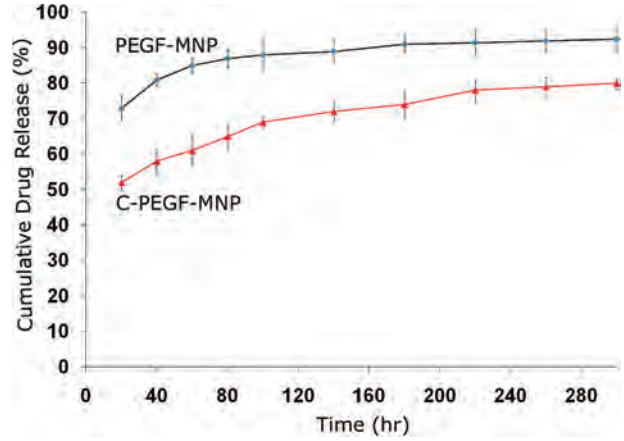

Figure 11. Release profile of tamoxifen from PEGF-MNP and C-PEGF-MNP over 12 days.

burst effects of 52% and 73%, respectively. The cross-linked C-PEGF-MNP were thus, as predicted, able to control the burst effect even in this very simple drug loading system. Better control over burst effect could be reached by additionally conjugating the drug to the C-PEGF-MNP.

3.4. Biocompatibility of SPIONs. Results of the MTT assays for L929 and K562 cells exposed to all SPION samples are shown in parts a and b of Figure 12, respectively. All synthesized SPION samples demonstrated acceptable levels of cell viability following exposure up to 400 mM, with none demonstrating toxic effects at the concentrations tested. In addition, the SPION with PEGF coating were more biocompatible than PVA coated SPION. Full details on PVA coated MNP are reported elsewhere.[34]

4. Conclusion

Poly(ethylene glycol) fumarate was synthesized from fumaryl chloride and polyethylene glycol in the presence of propylene glycol as a new proton scavenger and characterized as a rigid coating. The saturation magnetization of cross-linked nanoparticles was lower than noncross-linked and bare ones due to the lower amount of magnetite as well as magnetocrystalline anisotropy. TMX release from nanoparticles was studied. Effect of cross-linking reaction on the burst release was investigated. The study revealed that by introducing a cross-linking agent to the system, the burst effect was reduced by 21%. An MTT assay was used to investigate the biocompatibility of PEGF coated SPION of various molarities using L929 and K562 cells. All

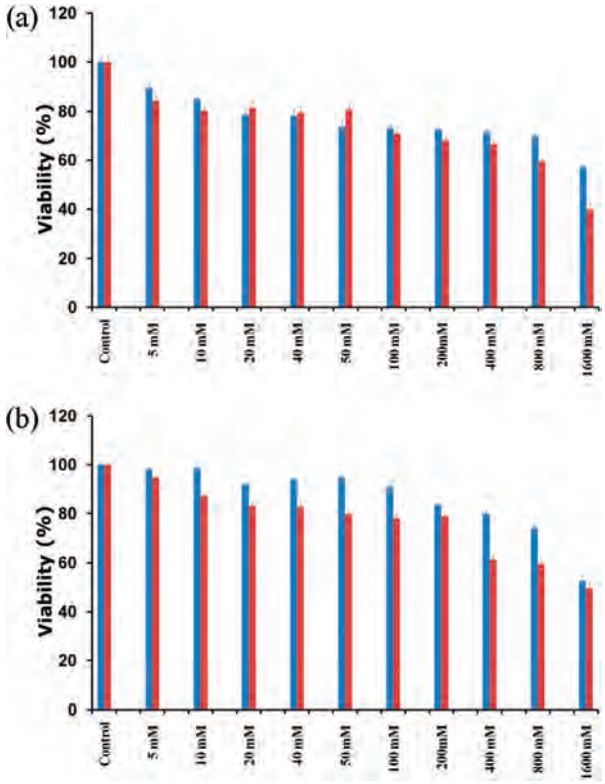

Figure 12. (a) MTT assay results for C-PEGF-MNP sample on (a) L929 and (b) K562 cells over 24 and 48 h.

compositions tested demonstrated acceptable levels of cell viability following exposures of up to 1600 mM iron concentration for up to 48 h. The obtained biocompatibility of PEGF-coated MNP was significantly larger than other polymeric coatings. Finally, the C-PEGF-MNP would be a very promising material for simultaneous diagnosis and therapeutic applications.

Supporting Information Available: Equation defining the polydispersity of the magnetic nanoparticles. This material is available free of charge via the Internet at http://pubs.acs.org.

References and Notes

(1) Häfeli, U. O. *The MML Series*; Kentus Books;: London, 2006; Vol. 8, pp 77−126.
(2) Flores, G. A.; Liu, *J. Eur. Cells Mater.* **2002**, *3* (2), 9–11.
(3) Tiefenauer, L. X. *Nanotechnology in Biology and Medicine: Methods, Devices, and Applications*; CRC Press: Boca Raton, FL,2007; pp 1−20.
(4) Olsvik, O.; Popovic, T.; Skjerve, E.; Cudjoe, K. S.; Hornes, E.; Ugelstad, J.; Uhlen, M. *Clin. Microbiol. Rev.* **1994**, *7*, 43–54.
(5) Gupta, A. K.; Curtis, A. S. G. *Biomaterials* **2004**, *25* (15), 3029–3040.
(6) Gupta, A. K.; Curtis, A. S. G. *Proc. 30th Annu. Symp. Controlled Release Bioact. Mater.* **2003**, *30*, 788.
(7) Gupta, A. K.; Berry, C.; Gupta, M.; Curtis, A. *IEEE Trans. Nanobiosci.* **2003**, *2* (4), 256–261.
(8) Widder, K. J.; Senyei, A. E.; Ranney, D. F. *Cancer Res.* **1980**, *40* (10), 3512–3517.
(9) Gupta, P. K.; Hung, C. T. *Microspheres and Regional Cancer Therapy*; CRC Press: Boca Raton, FL, 1993; pp 71−116.
(10) Gallo, J. M.; Hung, C. T.; Gupta, P. K.; Perrier, D. G. *J. Pharmacokinet. Biopharm.* **1989**, *17*, 305–326.
(11) Gallo, J. M.; Gupta, P. K.; Hung, C. T.; Perrier, D. G. *J. Pharm. Sci.* **1989**, *78*, 190–194.
(12) Zimmermann, U.; Vienken, J.; Pilwat, G. *Bioelectrochem. Bioenerg.* **1980**, *7*, 553–574.
(13) Freeman, J. A.; Geer, J. C. *Am. J. Dig. Dis.* **1965**, *10* (12), 1005–1025.
(14) Meyers, P. H.; Nice, J.; Meckstroth, G. R.; Becker, H. C.; Moser, P. J.; Goldstein, M. *Am. J. Roentgenol. Radium Ther. Nucl. Med.* **1966**, *96* (4), 913–21.
(15) Gupta, A. K.; Gupta, M. *Biomaterials.* **2005**, *26*, 3995–4021.
(16) Tchikov, V.; Winoto-Morbach, S.; Krönke, M.; Kabelitz, D.; Schütze, S. *J. Magn. Magn. Mater.* **2001**, *225*, 285–293.
(17) Krotz, F.; Sohn, H. Y.; Gloe, T.; Plank, C.; Pohl, U. *J. Vasc. Res.* **2003**, *40* (5), 425–434.
(18) Krotz, F.; de Wit, C.; Sohn, H. Y.; Zahler, S.; Gloe, T.; Pohl, U.; Plank, C. *Mol. Ther.* **2003**, *7* (5), 700–710.
(19) Häfeli, U.; Schütt, W.; Teller, J.; Zborowski, M. Plenum Press: New York, 1997.
(20) Berry, C. C.; Curtis, A. S. G. *J. Phys. D: Appl. Phys.* **2003**, *36*, 198–206.
(21) Moghimi, S. M.; Hunter, A. C.; Murray, J. C. *Pharm. Rev.* **2001**, *53*, 283–318.
(22) Harris, J. M.; Martin, N. E.; Modi, M. *Clin. Pharmacokinet.* **2001**, *40*, 539–551.
(23) Shu, X. Z.; Liu, Y.; Plumbo, F. S.; Luo, Y.; Prestwich, G. D. *Biomaterials* **2004**, *25*, 1339–1348.
(24) Sanborn, T. J.; Messersmith, P. B.; Barron, A. E. *Biomaterials.* **2002**, *23*, 2703–2710.
(25) Temenoff, J. S.; Shin, H.; Conway, D. E.; Engel, P. S.; Mikos, A. G. *Biomacromolecules* **2003**, *4*, 1605–1613.
(26) Ruel, G. E.; Leroux, J. C. *Eur. J. Pharm. Biopharm.* **2003**, *58*, 409–426.
(27) Jo, S.; Shin, H.; Shung, A. K.; Fisher, J. P.; Mikos, A. G. *Macromolecules* **2001**, *34*, 2839–2844.
(28) Timmer, M. D.; Jo, S.; Wang, C.; Ambross, C. G.; Mikos, A. G. *Macromolecules* **2002**, *35*, 4373–4379.
(29) He, X.; Ma, J.; Mercado, A. E.; Xu, W.; Jabbari, E. *Pharm. Res.* **2008**, *25* (7), 1552–1562.
(30) Park, H.; Temenoff, J. S.; Tabata, Y.; Caplan, A.; Mikos, A. G. *Biomaterials* **2007**, *28*, 3217–3227.
(31) Jordan, V. C. *Br. J. Pharmacol.* **2006**, *147*, 269–276.
(32) Pieters, R.; Huismans, D. R.; Leyva, A.; Veerman, A. J. P. *Br. J. Cancer.* **1989**, *59*, 217–220.
(33) Häfeli, U. O.; Pauer, G. J. *J. Magn. Magn. Mater.* **1999**, *194*, 76–82.
(34) Mahmoudi, M.; Shokrgozar, M. A.; Simchi, A.; Imani, M.; Milani, A. S.; Stroeve, P.; Vali, H.; Häfeli, U. O.; Sasanpour, P.; Bonakdar, S. *J. Phys. Chem. C.* **2009**, *113* (6), 2322–2331.
(35) Bolton, S. *Pharmaceutical Statistics: Practical and Clinical Applications*, 2nd ed.; Marcel Dekker: New York, 1990.
(36) Tasdelen, B.; Kayaman-Apohan, N.; Güven, O.; Baysal, B. M. *Polym. Adv. Technol.* **2004**, *15*, 528–532.
(37) Ibrahim, M. M.; Edwards, G.; Seehra, M. S.; Ganguly, B.; Huffman, G. P. *J. Appl. Phys.* **1994**, *75*, 15.
(38) Li, Y.; Liao, H.; Qian, Y. *Mater. Res. Bull.* **1998**, *33* (6), 841.
(39) Sun, J.; Zhou, S.; Hou, P.; Yang, Y.; Weng, J.; Li, X.; Li, M. *J. Biomed. Mater. Res., Part A* **2007**, *80*, 333–341.
(40) Haddad, P. S.; Martins, T. M.; Li, L. D.; Li, L. M.; Metze, K.; Adam, R. L.; Knobel, M.; Zanchet, D. *Mater. Sci. Eng., C* **2008**, *28*, 489–494.
(41) Huang, Z.; Tang, F. *J. Colloid Interface Sci.* **2005**, *281*, 432–436.
(42) Gomez-Lopera, S. A.; Plaza, R. C.; Delgado, A. V. *J. Colloid Interface Sci.* **2001**, *240* (1), 40–47.
(43) Jiang, W.; Yang, H. C.; Yang, S. Y.; Horng, H. E.; Hung, J. C.; Chen, Y. C.; Hong, C. Y. *J. Magn. Magn. Mater.* **2004**, *283*, 210–214.
(44) Mahmoudi, M.; Simchi, A.; Imani, M.; Milani, A. S.; Stroeve, P. *J. Phys. Chem. B* **2008**, *112* (46), 14470–14481.
(45) Godovsky, D. Y.; Varfolomeev, A. V.; Efremova, G. D.; Cherepanov, V. M.; Kapustin, G. A.; Volkov, A. V.; Moskvina, M. A. *Adv. Mater. Opt. Electron.* **1999**, *9*, 87–93.
(46) Ma, H. L.; Qia, X. R. *Int. J. Pharmacol.* **2007**, *333*, 177–186.

JP900798R